processes

MDPI

*Article*

# Experimental Characterization of Bimodal Granular Flow

**Lukáš Svoboda *, Tomáš Picek and Václav Matoušek ***

Faculty of Civil Engineering, Czech Technical University in Prague, Thákurova 7, 166 29 Prague 6, Czech Republic; tomas.picek@cvut.cz

* Correspondence: lukas.svoboda.2@fsv.cvut.cz (L.S.); v.matousek@fsv.cvut.cz (V.M.)

**Abstract:** Solid–liquid flows are encountered in various industrial and natural environments. The internal structure of such flows is highly sensitive to the grading of the solid particles present. In this experimental study, an extended stereometric method is employed to assess the distributions of velocity of particles of different fractions, distinguished by different colors, in vertical and nearly horizontal granular flows. In the vertical flow experiments, mixtures comprising three fractions of lightweight particles, characterized by a very similar density, size, and shape, were tested. The results affirmed the method's ability to discern particle velocity differences on the order of millimeters per second, establishing its suitability for characterizing nearly horizontal open-channel flows with bimodal mixtures that are stratified and exhibit more complex velocity distributions. Tilting flume experiments, incorporating additional measurements of water velocity distribution, allowed for the evaluation of local slip between water and particles, as well as between particles of the two fractions in the flow. The results indicated that, although the local slip velocity was relatively small, the average slip velocity between the carrying water and transported particles was significantly larger. This factor must be taken into consideration when evaluating bed friction or bed erosion for granular flow in a channel with an erodible bed.

**Keywords:** solid–liquid flow; intense sediment transport; velocity distribution; optical stereoscopic method; tilting flume experiment

check for updates

**Citation:** Svoboda, L.; Picek, T.; Matoušek, V. Experimental Characterization of Bimodal Granular Flow. *Processes* **2024**, *12*, 75. https://doi.org/10.3390/pr12010075

Academic Editor: Evangelos Tsotsas

Received: 29 November 2023
Revised: 21 December 2023
Accepted: 26 December 2023
Published: 28 December 2023

**Copyright:** © 2023 by the authors. Licensee MDPI, Basel, Switzerland. This article is an open access article distributed under the terms and conditions of the Creative Commons Attribution (CC BY) license (https://creativecommons.org/licenses/by/4.0/).

## 1. Introduction

Granular flows manifest as physical processes in various industries and natural environments. Flows involving mixtures of liquid and solid particles span a broad spectrum of conditions, displaying complex behaviors that are challenging to describe and model.

### *1.1. Granular Flows in Conduits*

Two types of granular flow are distinguished based on the conduit through which granular mixtures flow. One type is the flow in pressurized pipes, primarily driven by the difference in static pressure across different cross sections of a pipe. In the other type of granular flow, no pressure difference exists between flow cross sections, and the flow is driven by gravity. This type is known as open-channel flow.

#### 1.1.1. Solid–Liquid Flow in Pressurized Pipes

Pipeline transport of solids in a flowing liquid carrier is widely employed across various industries, including mining, dredging, oil and gas, chemistry, agriculture, and waste treatment [1–3]. The diverse industrial applications of hydraulic transport necessitate the pumping and conveyance of very different solid–liquid mixtures through pipelines.

The granular flows of interest in this paper are aqueous mixtures of relatively coarse particles that tend to settle and stratify from the carrier within the pipeline—commonly referred to as settling slurry flows. In these flows, the carrying liquid and solid particles interact, influencing the behavior of the mixture flow. Settling slurry flows are typically turbulent, with solid particles interacting with turbulent eddies in the flowing carrier.

Additionally, interparticle collisions or longer-lasting contacts further contribute to the interactions [4,5].

These interactions result in an alteration in the internal structure of the flow, leading to an asymmetrical distribution of velocity and a non-uniform distribution of solids across the cross-section of the pipe. This alteration is particularly pronounced when the concentration of solids in the mixture is high. Understanding the internal structure of solid–liquid flow is crucial for identifying the flow behavior within a pipe.

#### 1.1.2. Solid-Liquid Flow in Open Channel

Highly concentrated solid–liquid flows also occur in open channels, commonly associated with the transport of sediment in mobile-bed rivers and streams. This sediment transport becomes particularly pronounced during extreme flow conditions, such as flash floods in mountain streams. For an accurate understanding of intense sediment transport in an open channel, it is crucial to determine the distributions of sediment and its velocity within the turbulent flow of the carrying water.

### *1.2. Experimental Characterization of Granular Flows in Laboratory Set-Ups*

A comprehensive experimental characterization of granular flows necessitates information on the distribution of solid particles and their local velocities throughout the flow. This information is essential not only for understanding the flow itself but also for validating predictive models for solids-laden flows in conduits. In controlled laboratory conditions, advanced measuring techniques are available to assess these distributions in both pressurized pipes and open channels.

In laboratory pipe loops, measuring techniques encompass electric tomography methods and radiometric methods, among others. A survey of the most frequently used methods can be found in works such as ref. [6]. While these methods are successful in identifying the distributions of total solids, they may fall short in distinguishing between different fractions that vary in size or any other property within the total population of solids.

In laboratory flumes, acoustic Doppler measuring techniques have been frequently employed to detect solids velocity distributions. Model lightweight solids are often used to facilitate ultrasonic sensing of distributions in high-concentration solid–liquid flows, mimicking the intense transport of mono-sized sediment in an open channel, e.g., refs. [7–10]. An alternative method for measuring velocity distribution in highly concentrated sediment-laden flow utilizes an optical approach, e.g., refs. [11–15]. This method employs stereoscopy, tracking individual particles through a set of two high-speed cameras that sense the flow through a transparent sidewall of the flume [16,17].

We have successfully applied the stereoscopic method to measure the velocity distributions in turbulent flows carrying lightweight mono-sized sediments in a laboratory tilting flume [14,18,19]. The stereoscopic method relies on the presence of identical particles, ensuring reliable identification of the particle locations obtained from greyscale images produced by the cameras.

To apply the method and its principles to particles of different properties transported together in one flow, modification and further development of the identification technique are required to account for differences in particle properties. This modification is also necessary for bimodal granular flows, involving solids of two fractions differing in particle size.

### *1.3. Experimental Testing of Bimodal Granular Flows*

Bimodal granular flows exhibit specific behaviors that differ from the behavior of unimodal granular flows and have practical consequences. When the two fractions of a bimodal mixture significantly differ in size, the bimodal flow tends to stratify, impacting flow friction and transport capacity.

In industrial pipes transporting settling slurries, the size of a solid particle is a key parameter affecting the behavior of solid–liquid slurry flow. It is generally accepted

that a considerable reduction in friction loss can be achieved by transporting broadly graded solids instead of uniformly graded solids of the same mass–median grain size [20]. This effect has been studied experimentally in laboratories primarily for bimodal slurries composed of two narrow-graded fractions of solids [21–25].

As highlighted in previous studies (e.g., [26]), the difference in friction loss is particularly significant in slurries that are stratified. In stratified bimodal slurries, finer particles can reduce the mechanical friction associated with the sliding of coarser particles over a pipe wall by developing a thin layer, effectively separating the coarse particles from the pipe wall.

In open channels with mobile beds, the beneficial impact of transporting sediment with broad grading on channel capacity has been observed [27–31]. A recent laboratory study involving a model bimodal sediment composed of two fractions of spherical glass beads confirmed this effect [32,33]. The experiment focused on the effects of adding fine particles to a flow transporting coarser particles. The flume was supplied with constant flow rates of water and solids. The addition of the fine fraction enhanced the transport of the coarse fraction and reduced the equilibrium longitudinal slope of the bed. The study revealed that the stratification of the fractions, leading to the development of a layer composed of particles of the fine fraction at the top of the mobile bed over which particles of the coarse fraction moved, was responsible for the reduction in friction.

Our experimental investigations concentrated on bimodal flows with a higher bed shear, resulting in significantly more intense transport compared to the aforementioned experiment [34]. These experiments revealed segregation due to kinetic sieving and the development of a layered structure in the bimodal mixture flow. In this structure, a thick transport layer was separated from the top of the bed by an interfacial layer of fine particles. The transport of the coarser fraction dominated, with more than two-thirds of the total volume of transported particles occupied by the coarse fraction. As a result, an increase in the velocity gradient across the transport layer and a decrease in the interfacial friction coefficient were observed in bimodal flow compared to the corresponding unimodal coarse flow under hydraulically similar conditions [35].

To incorporate measurements of velocity distributions for particles of two fractions into our experimental characterization of bimodal granular flows in a laboratory flume, we recently modified the optical stereoscopic method [36]. This modification extended its capabilities by allowing the recognition and separation of particles that differ in color before the method tracks the particles and determines their local velocities. The enhanced method's capabilities were assessed in an experiment involving a bimodal mixture composed of nearly spherical particles from two fractions with very similar sizes and densities, conducted in a simple vertical flow [36]. Further refinement of this evaluation is necessary to include more fractions and gather additional information about the flow used for testing the method.

### *1.4. Scope and Structure of This Paper*

We present an experimental characterization of open-channel granular flow carrying solids at high concentrations above a mobile granular bed. The challenge lies in separating the information on the velocity distributions of the two fractions in the flowing bimodal mixture.

## 2. Experimental Work: Materials and Methods

Two sets of laboratory experiments were conducted at the Water Engineering Laboratory of Czech Technical University in Prague. The first set aimed to test and refine the capabilities of the extended stereoscopic method. This was achieved using a recirculating cell with a vertical measuring section. In the second set of experiments, the method was applied to open-channel flow with intense transport of bimodal solids. These experiments took place in a recirculating tilting flume.

### *2.1. Laboratory Set-Ups and Measuring Techniques*

#### 2.1.1. Recirculating Vertical Cell

The vertical recirculating cell, utilized in preceding tests [36], underwent a comprehensive remodeling for the new tests. A schematic sketch of the updated cell is presented in Figure 1.

The recirculating loop comprises two vertical pipes (Figure 1). The PVC pipe, denoted as No. 1 in Figure 1, features a circular cross-section. Within this pipe, there is a section equipped with two propellers (No. 2) attached to a shaft driven by an electric motor (No. 3), which offers variable frequency options. The upper end of this vertical pipe is sealed by a horizontal sieve (No. 4), preventing particle leakage from the loop and facilitating the overflow of excess water in case the loop volume is filled with particles. The system ensures the safe removal of overflowing water through a piping connected with the overflow (No. 11). Additionally, a magnetic flow meter (No. 12) with an 80 mm internal diameter is mounted to the vertical pipe.

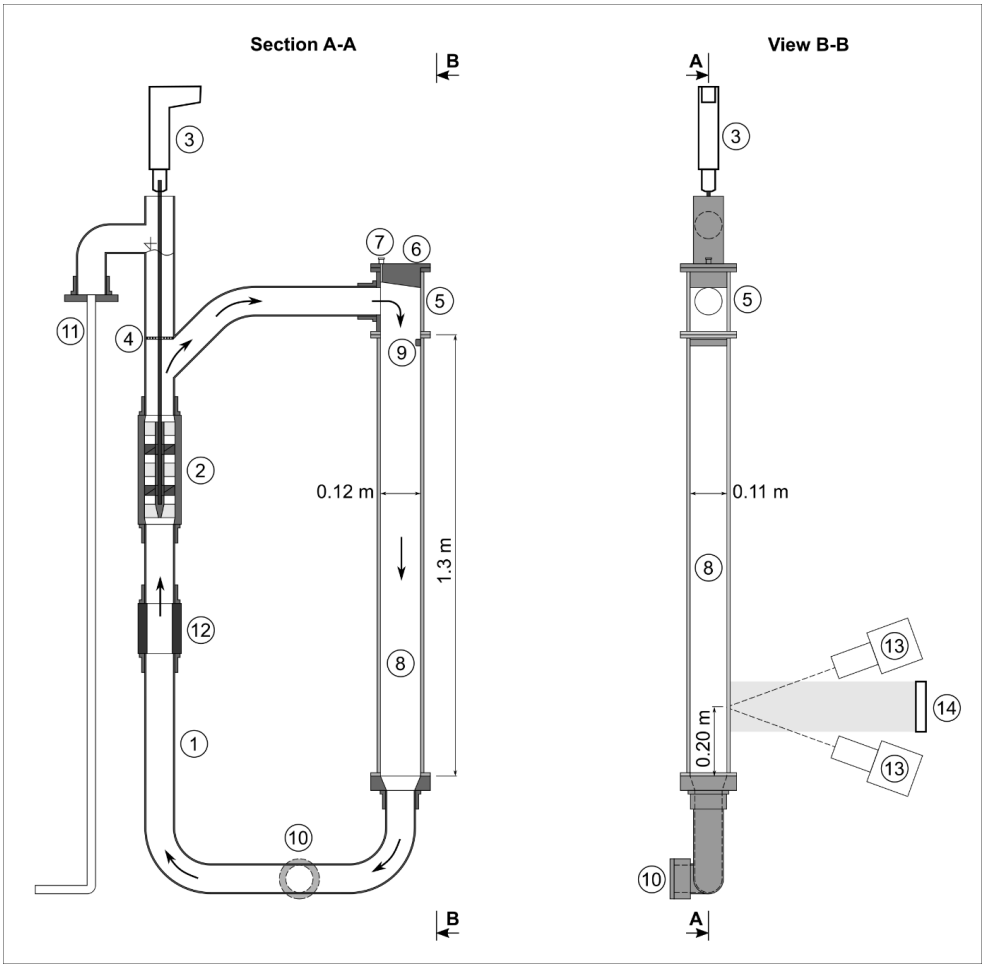



**Figure 1.** Recirculating vertical cell with measuring equipment. Legend: 1. PVC pipe, 2. two propellers fixed on shaft, 3. electric motor, 4. horizontal sieve, 5. inlet pipe fitting, 6. hatch, 7. air release valve, 8. plexiglass pipe, 9. flow-directing sill, 10. Invert U-bend with hatch, 11. overflow pipe, 12. flow meter, 13. high-speed cameras, 14. lighting system.

The other vertical pipe (No. 8), constructed from transparent plexiglass, has a rectangular cross-section with internal dimensions of 0.12 × 0.11 m and a length of 1.3 m. Serving as a measuring section, this pipe is attached to the inlet piece, which incorporates a fitting (No. 5) for inserting a calibration plate. The inlet piece includes a lid (No. 6), an air release valve (No. 7) for the removal of air bubbles, and a flow-directing deflector (No. 9)

for enhanced homogenization and alignment of the mixture at the inlet to the measuring section. A valve (No. 10) in the invert U-bend connecting the two vertical pipes allows for the complete emptying of the system.

Particles in the downward flow through the measuring section are tracked using a pair of FASTCAM Mini AX50 high-speed cameras (No. 13); specifically, model 170K-C-32 with a 50 mm lens. These cameras are vertically mounted to the cell frame and focused on the center of the cross-section, positioned 0.2 m above the measuring section outlet. The cameras are set at an angle of 40° between them and are placed 0.375 m from the transparent wall of the measuring section.

An Amaran Tri-8s LED lighting system (No. 14), positioned between the cameras at a right angle to the center of the high-speed camera focus, facilitates the adjustment of different aperture counts. A larger aperture count is employed to achieve a greater depth of field (DOF), ensuring improved image clarity of all visible particles in the flow.

#### 2.1.2. Measuring Procedures in the Recirculating Vertical Cell

The pair of high-speed cameras enables stereometric recording of particle movement through the transparent wall of the measuring section in the vertical cell. Before conducting stereoscopic measurements, a calibration image is taken for each of the two cameras to ensure proper conversion of the coordinate system of images in pixels into the coordinate system in millimeters.

White-color calibration of the high-speed cameras is performed before each measurement to ensure consistency in color capturing for all measurements. A plate of white color is placed in the view field of both cameras and illuminated the same way the measuring section is illuminated during measurements. The white balance function is activated, and it adjusts the camera settings so that the white plate is recorded as pure white.

Subsequently, the cameras are set to record images at a frame capture rate of 1000 frames per second and at an f-number J. This setting ensures that the collected images are sufficiently sharp, and the maximum displacement of a particle in two consecutive frames does not exceed one diameter of the particle.

The collected images undergo cropping to eliminate the sidewalls of the pipe. This step is succeeded by an analysis of the hue boundaries for the colors of the particle fractions, utilizing a statistical method known as cluster analysis. The analysis-based boundary values are checked and, if necessary, slightly adjusted to ensure that only particles of the particular color are included in the adjusted images. Three fractions of different colors were used in the cell tests, and the optimized values of their hue boundaries are given in Table 1.

**Table 1.** Properties of plastic particles used in the recirculating cell.

| | **PGR** | **PGG** | **PGB** |
|---|---|---|---|
| Color | Red | Green | Blue |
| Size [mm] | 5.95 | 5.91 | 5.92 |
| Density [kg/m$^3$] | 1005 | 1018 | 1021 |
| Terminal settling velocity in water [mm/s] | 23.0 | 43.6 | 47.5 |
| Optimized hue boundaries | [0, 0.16; 0.95, 1] | [0.16, 0.50] | [0.50, 0.95] |

Sets of images are generated for individual fractions by separating their particles using the respective hue ranges for fraction colors. In each set, the edited images display only the particles of the fraction color, and the rest of the image is black. This procedure results in three sets of images, enabling separate evaluation of particle motion for the three fractions. The images of each set are ultimately converted to grayscale for further processing using the stereoscopic method. The stereoscopic processing produces the velocities of the particles for the three fractions separately.

2.1.3. Recirculating Tilting Flume

The recirculating tilting flume has dimensions of 200 mm in width, 8 m in length, and a measuring section that spans 6 m. The flume is designed to be tilted over a broad range of longitudinal slopes. A comprehensive description of the setup, measuring techniques, and experimental procedures can be found in previous publications [8,14]. The setup is equipped with measuring instruments to gather information on the total discharge (the discharge of the mixture of liquid and solids), discharge of solids, and the elevation of the water surface along the flume.

The total flow rate is measured using a magnetic flow meter, and the solid flow rate is obtained from the average delivered concentration acquired through differential-pressure measurements in an inverted vertical U-tube, which is part of the recirculating loop. The elevation of the water surface along the flume is monitored by a set of ultrasonic level meters (Figure 2). The positions of the top of the bed at the bottom of the flume are observed visually, obtained from video images, and alternatively derived from the distributions of velocity and concentration across a flow cross-section (e.g., [37]).

To evaluate the uniformity of the flow essential for the experiments, ultrasonic level meters are employed to measure the water level at five points. In cases of non-uniform flow, adjustments are made to controllable parameters, such as the flow rate, flume slope, or the height of the sluice gate at the flume outlet (Figure 2).

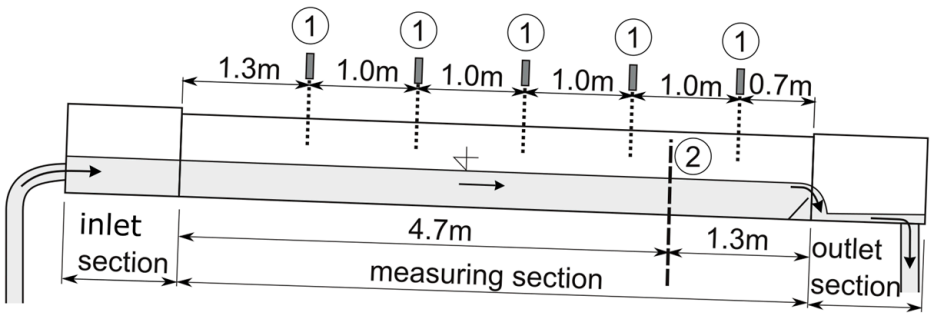



**Figure 2.** Set-up of ultrasonic level meters and location of measuring cross section in the tilting flume. Arrows indicate flow direction through the flume. Legend: 1. ultrasonic level meters, 2. measurement cross section for stereoscopic method and for Prandtl tube.

2.1.4. Measuring Procedures in the Tilting Flume

The high-speed cameras were set up in the same manner as in the vertical cell experiment. Positioned horizontally next to each other at a mutual angle of 40° and 380 mm from the transparent sidewall of the flume (Figure 3), the cameras were focused on the cross-section where the velocity distribution was measured using a Prandtl tube (Figure 2). The same light source used in the cell experiment was placed between the cameras. Prior to each measurement, white-color calibration was performed, and a calibration image was captured following the same procedure as in the vertical cell experiment.

Due to the higher flow velocities than in the vertical cell, the cameras were set to record images at a rate of 2000 frames per second instead of 1000 frames per second for the cell tests. The f-number was J. The optimized values of the hue boundaries for the two fractions of solids used in the flume tests are given in Table 2.

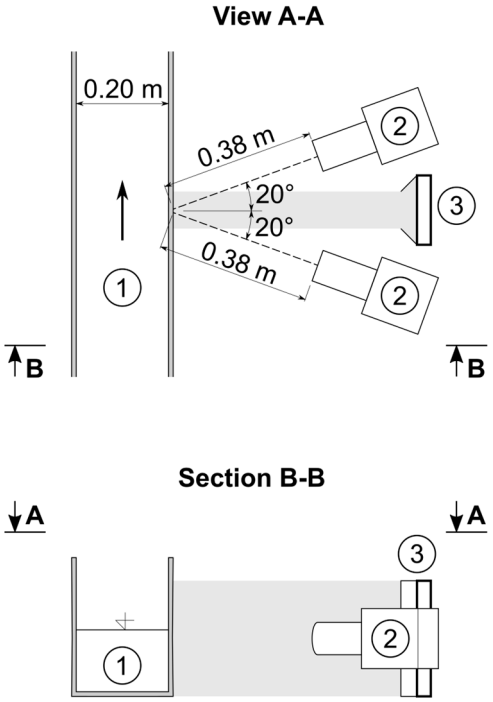



**Figure 3.** Set-up of cameras in the tilting flume. Legend: 1. flume, 2. FASTCAM Mini AX50 high-speed cameras, 3. an Amaran Tri-8s LED lighting system.

**Table 2.** Properties of lightweight solids used in the tilting flume.

| | **SUN25** | **FA30** |
|---|---|---|
| Color | Red | Green |
| Shape | Prism | Lens |
| Size [mm] | 2.8 | 3.65 |
| Density [kg/m$^3$] | 1280 | 1368 |
| Terminal settling velocity in water [mm/s] | 76.5 | 114 |
| Optimized hue boundaries | [0.0, 0.19; 0.99, 1] | [0.19, 0.99] |

The Prandtl tube measured the local velocities of the water in the center of the measuring cross-section (e.g., 100 mm from the side walls), and the tube was shifted along the flow depth to sense the velocity distribution between the bed and the water surface. The stereoscopic method captured the velocity distributions of the particles in each fraction near the sidewall in the same cross-section of the flume.

### *2.2. Tested Solids*

For the experiments in the vertical cell, three fractions of nearly spherical plastic particles were employed. These fractions were distinguished by their color (see Figure 4), and the particles of the chosen fraction had a very similar size and density to prevent segregation in the vertical flow (Table 1). Additionally, the particles were designed to be nearly neutrally buoyant, reducing the slip caused by differences in local velocities between particles and water in the vertical flow of the mixture.

The density, size, and terminal settling velocity of the particles from the three fractions were determined experimentally. Due to the density of the plastic particles, which was similar to the density of water, the settling experiments were conducted in both water and petrol to encompass a broad range of settling velocities. The results of these settling tests facilitated the calibration of the particle shape factor for use of the Haider–Levenspiel predictive method [38]. A suitable value for all three fractions was determined to be 0.94, indicating a shape very similar to a sphere. The settling velocity values obtained using the Haider–Levenspiel method, with the calibrated shape factor, are presented in Table 1.

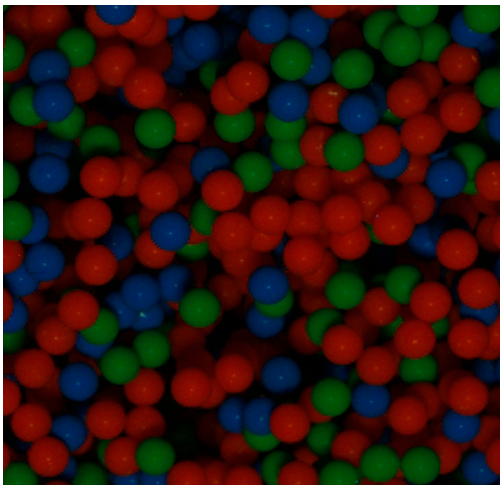


**Figure 4.** Image of mixture of particles PGR, PGG, and PGB in the vertical flow of a recirculating cell.

Two fractions of strongly non-spherical lightweight sediment, coded as FA30 and SUN25, comprised of plastic particles that were virtually mono-sized, were combined in a bimodal mixture in the flume (Figure 5). In addition to varying particle shapes, the two fractions differed in physical properties and color (see Table 2). These fractions had been previously employed in flume tests with unimodal sediments [18,19,37], and their physical properties were determined experimentally.

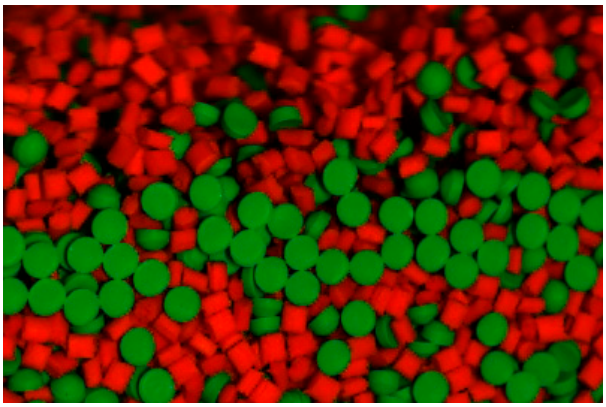


**Figure 5.** Image of mixture of particles FA30 and SUN25 in the nearly horizontal flow in a tilting flume.

Particles from the two fractions were mixed in approximately equal volume proportions, with one-half of the total volume occupied by FA30 particles and the other half by SUN25 particles. This combination resulted in a bimodal sediment (coded as FAS), which was then introduced into the recirculating flume system.

### *2.3. Experiment in the Recirculating Cell*

The vertical flow in the recirculating cell provided suitable conditions for testing and optimizing the capabilities of the extended stereoscopic method in tracking particles of different fractions. This vertical flow is simple, in the sense that the transported particles do not stratify across the flow cross-section of the pipe and do not tend to collide with each other or with the pipe wall. Instead, particles from all three fractions are almost uniformly distributed across the pipe, primarily interacting with the carrying liquid. These uncomplicated conditions of mixture flow enabled a relevant experimental comparison of fraction behaviors and their theoretical predictions.

The primary goal of testing the method was to evaluate and, if possible, optimize the procedure, which involves dividing a source (unedited) image produced by a camera into

filtered images, each displaying particles of just one of the multiple (in this case, three) fractions based on the corresponding hue. This process results in a reliable determination of local velocities for particles of each fraction separately.

A total of 22 test runs were conducted, including four series of tests, each with a certain constant proportion of solids fractions in the mixture. Within each series, mixtures with different total volume concentrations of solids were tested at two different flow velocities (Table 3).

**Table 3.** Test runs with a trimodal mixture composed of fractions PGG (G), PGR (R), and PGB (B) in a recirculating cell. Flow velocity measured using a magnetic flowmeter, $v_{flow}$; volume concentration of solids in the mixture, $C_v$; cross-section-averaged velocity of particles PGG, $v_{PGG}$; cross-section-averaged velocity of particles PGR, $v_{PGR}$; cross-section- averaged velocity of particles PGB, $v_{PGB}$.

| Run No. | $v_{flow}$ (m/s) | $C_v$ (%) | RatioG/R/B | $v_{PGG}$ (m/s) | $v_{PGR}$ (m/s) | $v_{PGB}$ (m/s) |
|---|---|---|---|---|---|---|
| 1 | 0.205 | 8.72 | 25/50/25 | 0.212 | 0.200 | 0.214 |
| 2 | 0.417 | 8.72 | 25/50/25 | 0.399 | 0.388 | 0.395 |
| 3 | 0.197 | 17.43 | 25/50/25 | 0.206 | 0.191 | 0.205 |
| 4 | 0.409 | 17.43 | 25/50/25 | 0.39 | 0.386 | 0.397 |
| 5 | 0.212 | 26.15 | 25/50/25 | 0.176 | 0.161 | 0.176 |
| 6 | 0.409 | 26.15 | 25/50/25 | 0.384 | 0.378 | 0.385 |
| 7 | 0.205 | 8.71 | 50/25/25 | 0.228 | 0.218 | 0.230 |
| 8 | 0.42 | 8.71 | 50/25/25 | 0.412 | 0.406 | 0.409 |
| 9 | 0.201 | 17.42 | 50/25/25 | 0.207 | 0.200 | 0.208 |
| 10 | 0.405 | 17.42 | 50/25/25 | 0.354 | 0.359 | 0.364 |
| 11 | 0.189 | 26.13 | 50/25/25 | 0.145 | 0.142 | 0.151 |
| 12 | 0.402 | 26.13 | 50/25/25 | 0.342 | 0.346 | 0.348 |
| 13 | 0.212 | 10.86 | 25/25/50 | 0.212 | 0.210 | 0.221 |
| 14 | 0.417 | 10.86 | 25/25/50 | 0.419 | 0.414 | 0.419 |
| 15 | 0.205 | 21.73 | 25/25/50 | 0.195 | 0.188 | 0.194 |
| 16 | 0.409 | 21.73 | 25/25/50 | 0.371 | 0.357 | 0.367 |
| 17 | 0.197 | 8.73 | 33/34/33 | 0.207 | 0.195 | 0.210 |
| 18 | 0.409 | 8.73 | 33/34/33 | 0.422 | 0.411 | 0.420 |
| 19 | 0.205 | 17.47 | 33/34/33 | 0.196 | 0.186 | 0.200 |
| 20 | 0.402 | 17.47 | 33/34/33 | 0.366 | 0.365 | 0.371 |
| 21 | 0.212 | 26.20 | 33/34/33 | 0.178 | 0.172 | 0.183 |
| 22 | 0.402 | 26.20 | 33/34/33 | 0.350 | 0.347 | 0.352 |

### *2.4. Experiment in the Tilting Flume*

When transported in the water flow through the flume, particles from the two fractions exhibited a tendency to stratify and form a transport layer above a stationary granular bed that occupies the bottom of the flume. Figure 6 presents a photograph capturing the flow in the flume, taken through a transparent sidewall. In the photo, the dashed blue line delineates the visually observed top of the stationary bed, while the parallel black line marks the top of the transport layer beneath the water surface; both are visible in the image. The ruler affixed to the sidewall, with zero at the bottom of the flume, indicates elevations of the interfaces and the water surface. While particles from both fractions were present in both the bed and the transport layer, a greater number of coarser fraction particles (green particles) tended to occupy the bed compared to the finer fraction particles (red particles). Conversely, in the transport layer, the proportions were reversed.

Two tests conducted for the bimodal mixture are presented. The two tested flows had very similar water flow rates, $Q_f$, and differed in the flow rates of solids, $Q_s$ (Table 4). The results of the solids flow rates determined experimentally using two independent methods exhibited very reasonable agreement. The total flow rate, $Q_m$, measured using a magnetic flow meter, is the sum of $Q_f$ and $Q_s$. The delivered volumetric concentration, $C_{vd}$, defined as $C_{vd} = Q_s/Q_m$, is a suitable measure of the intensity of solids transport, and it was higher in Test No. 2.

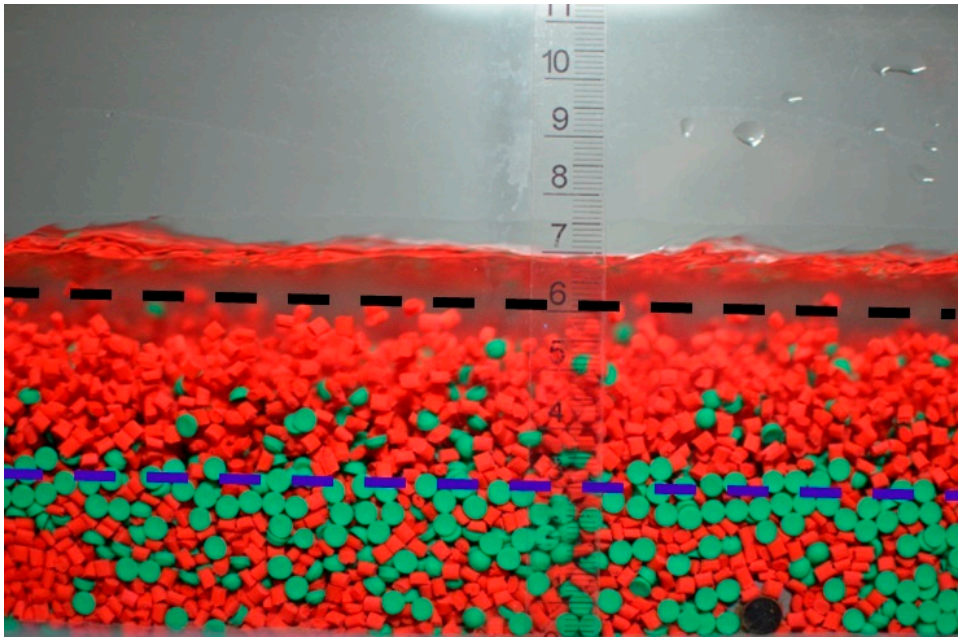



**Figure 6.** Bimodal transport of lightweight sediment in tilting flume (Test No. 1). Legend: blue line—visually observed elevation of the top of the stationary bed, black line—visually observed elevation of the top of the transport layer.

**Table 4.** Cross-section-averaged quantities obtained from the experiments.

| Quantity [Unit] | Test No. 1 | Test No. 2 |
|---|---|---|
| Flow rate of water $Q_f$ [L/s] | 5.69 | 5.81 |
| Flow rate of solids $Q_s$ via U-loop [L/s] | 0.44 | 0.71 |
| Flow rate of solids $Q_s$ via sampling [L/s] | 0.41 | 0.69 |
| Total flow rate $Q_m$ via magnetic flow meter [L/s] | 6.11 | 6.51 |
| Delivered concentration $C_{vd}$ via U-loop [−] | 0.072 | 0.109 |
| Delivered concentration $C_{vd}$ via sampling [−] | 0.067 | 0.107 |

## 3. Results and Discussion

### *3.1. Experimental Results from Recirculating Cell*

#### 3.1.1. Local and Average Velocities of Particles of Different Fractions

The vertical velocity distributions of the particles from the different fractions were obtained from the camera images processed using the extended stereoscopic method. Subsequently, the cross-section-averaged velocities were derived from these distributions. Table 3 compiles the average vertical velocities for all three fractions across 22 test runs. The results demonstrate a very reasonable agreement with the average flow velocity measured using the magnetic flow meter. Additionally, a deviation is observed in the average velocities of the three fractions, indicating that the average particle velocity of the red fraction ($v_{PGR}$) is less than the average particle velocity of the green fraction ($v_{PGG}$), and it is also less than the average particle velocity of the blue fraction ($v_{PGB}$) (Figure 7).

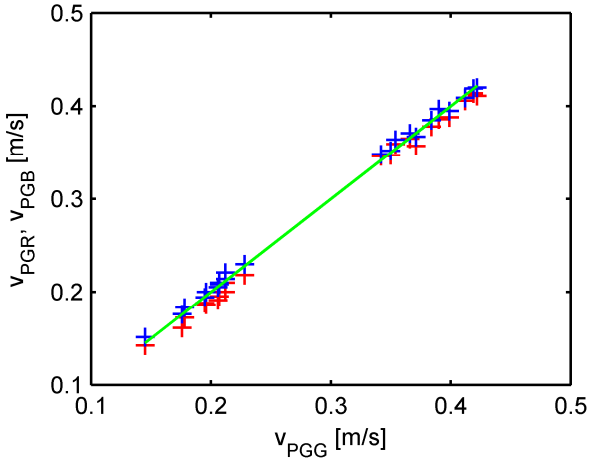



**Figure 7.** Cross-section-averaged velocities of particles of different fractions in the vertical measuring section of the recirculating cell. Red + = measured particle velocity of PGR ($v_{PGR}$); blue + = measured particle velocity of PGB ($v_{PGB}$); green line = measured particle velocity of PGG ($v_{PGG}$).

### 3.1.2. Average Slip Velocity between Fractions in Vertical Flow

Interestingly, the difference in the average vertical velocity between the particles from the two fractions correlates remarkably well with the difference in the hindered settling velocity of these particles, calculated using the Haider–Levenspiel method and including the hindered effect using the Richardson–Zaki method [39] (Figure 8). The settling velocity serves as a reliable indicator of the average slip velocity, defined as the difference between the liquid velocity and solid velocity, in the vertical granular flows where the particles do not collide with each other and primarily interact with the flowing carrier (e.g., ref. [6]).

This result underscores the capability of the extended stereoscopic method to effectively separate the particles of the different fractions and discern subtle differences in their velocities, even when these differences are on the order of millimeters or lower tens of millimeters per second.

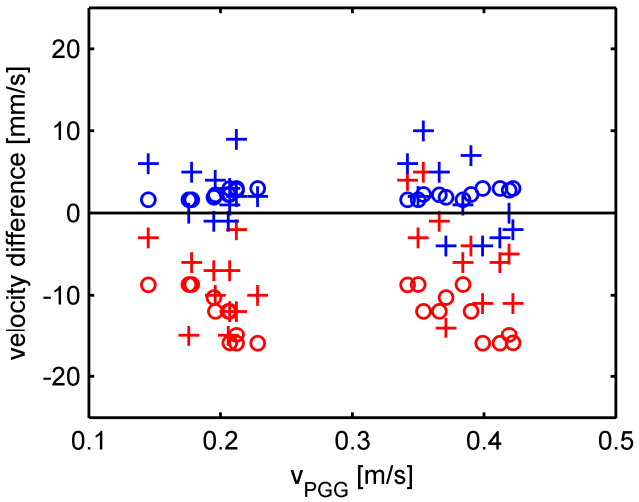



**Figure 8.** Differences in the cross-section-averaged velocities of the particles. Red o = measured difference in the particle velocities of fractions PGR and PGG ($v_{PGR} - v_{PGG}$); red + = calculated difference in the hindered settling velocity of fractions PGR and PGG; blue o = measured difference in the particle velocities of fractions PGB and PGG ($v_{PGB} - v_{PGG}$); blue + = calculated difference in the hindered settling velocity of fractions PGB and PGG.

### *3.2. Experimental Results from the Tilting Flume*

In contrast to the vertical flows tested in the recirculating cell, the nearly horizontal flows in the tilting flume exhibit a tendency to stratify, resulting in a non-uniform distribution of transported solids across the flow depth. This distribution shows higher local concentrations of the solids near the bed and lower concentrations below the water surface, as demonstrated by previously measured distributions of SUN25 solids from an experiment with unimodal granular flow in the flume [19]. The distribution of solids significantly influences the local velocities and alters the velocity profiles for both the water and solids across the flow depth.

#### 3.2.1. Application of the Stereoscopic Method in the Granular Flow in the Flume

A comprehensive explanation of the stereoscopic image analysis method and its application in granular flow in a laboratory flume is provided in refs [12,16,17]. Stereoscopic imaging allows for the acquisition of 3D particle positions using Voronoi diagrams, facilitating the stereoscopic matching of particles and enabling pattern-based particle tracking. The use of Voronoi diagrams for 2D particle tracking is detailed in ref. [16], and its extension to 3D is discussed in ref. [17]. Examples of the resulting trajectories and vectors of moving particles in granular flow through a flume can be found in refs. [12,15], along with a discussion of method limitations, uncertainties, and errors in flume applications.

Errors in particle velocities primarily result from uncertainties in determining particle locations, but these tend to cancel out when the time-averaged velocity profile is estimated from a large set of measurements [15]. Time-averaging of the local particle velocity is performed in a control volume given by a nearly horizontal layer, which is between one and two particle sizes thick. This time-averaging method is suitable for steady uniform flow in the flume. It is important to note that our extension of the stereoscopic method to multi-species granular flows does not alter the fundamental procedures of the method.

In this paper, we are particularly interested in time-averaged velocities. In our processing, the time-averaged velocity is calculated from a sample of 1000 frames. Figure 9 provides an example of particle trajectories from which particle velocities are obtained for both solid fractions. Figure 10 shows the resulting average velocity profiles.

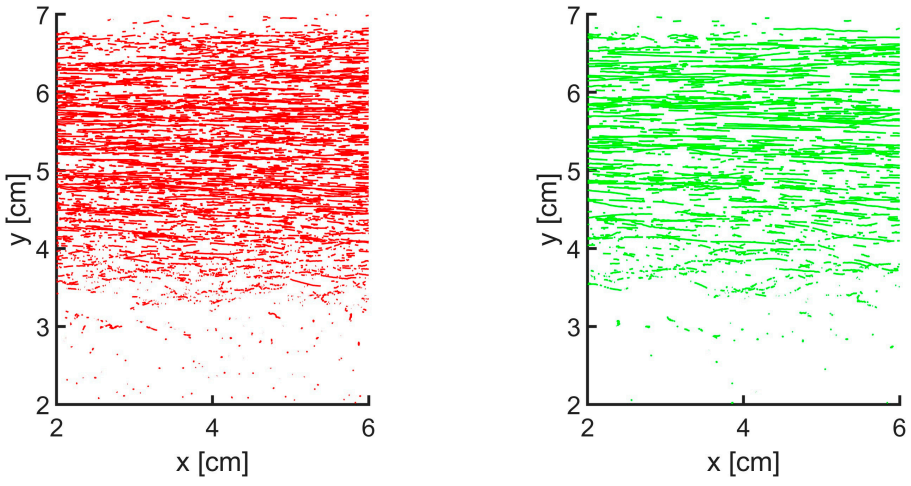



**Figure 9.** Particle trajectories derived from 250 successive frames using the Voronoi-based particle tracking algorithm for particles of two fractions in the bimodal granular flow in the tilting flume (test no. 1). **Left**: SUN25 particles; **right**: FA30 particles.

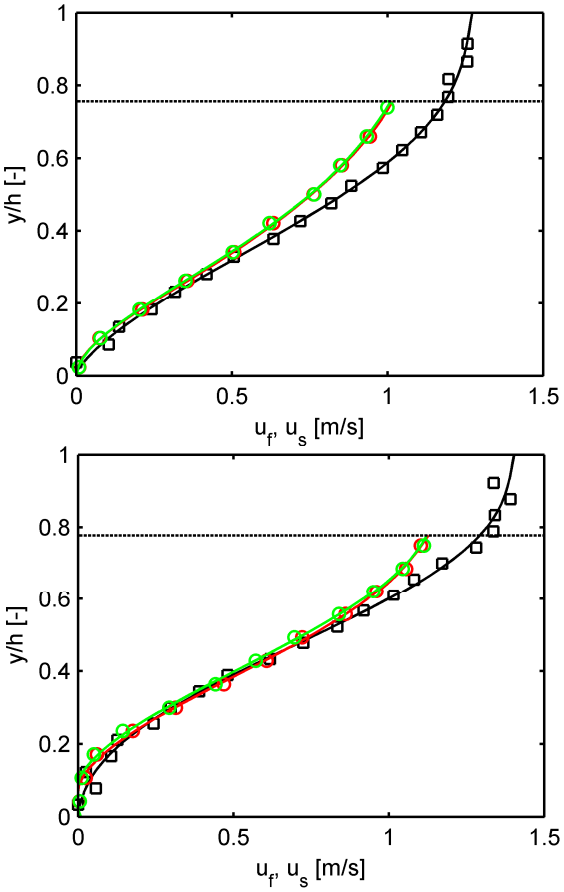



**Figure 10.** Distributions of the local velocities of the particles and water across flow depth in the tilting flume. **Upper plot**: test no. 1, **lower plot**: test no. 2. Legend: horizontal bottom line—top of the stationary bed; horizontal top line—water surface; horizontal dash line—top of the transport layer; black marker—velocity of water measured by the Prandtl tube; red marker—velocity of SUN25 particles measured using the stereoscopic method; green marker—velocity of FA30 particles measured using the stereoscopic method; curves—polynomial approximation of the measured values.

### 3.2.2. Local Velocity and Local Slip in Flume

Figure 10 compares the measured distributions of the time-averaged longitudinal velocities of the water ($u_f$) and particles ($u_s$) for the two fractions in the tested bimodal mixture (refer to the tests in Table 4). The local water velocities are determined at various elevations across the entire flow depth ($0 < y/h < 1$), while the local velocities of the particles are determined within the transport layer only.

The local velocities differ slightly at the same elevation above the bed across the flow depth, indicating that the local slip exists. There is a local lag between the velocity of the particles and that of the water. Also, there is local lag between the velocity of the coarser particles (FA30) and that of the finer particles (SUN25). In general, the local slip velocities are small. Note that the detected increase in the local slip velocity between the water and the particles at the elevations near the top of the transport layer may be an artifact caused by uncertainty in the detection of the particle velocity using the stereoscopic method in this region where the local concentration of the particles is low. The hypothesis that the stereoscopic method produces a local particle velocity that is too low in the region containing a low concentration of solids is supported by the observation that the difference is smaller in test no.2, where the local concentrations in the transport layer are higher than in test no. 1.

Figure 11 shows that the local slip velocity between SUN25 particles and FA30 particles is in the order of lower tens of millimeters per second in both tests. The plotted local slip

velocity is the difference in the local velocity of each fraction determined by the polynomial approximation, as shown in Figure 10.

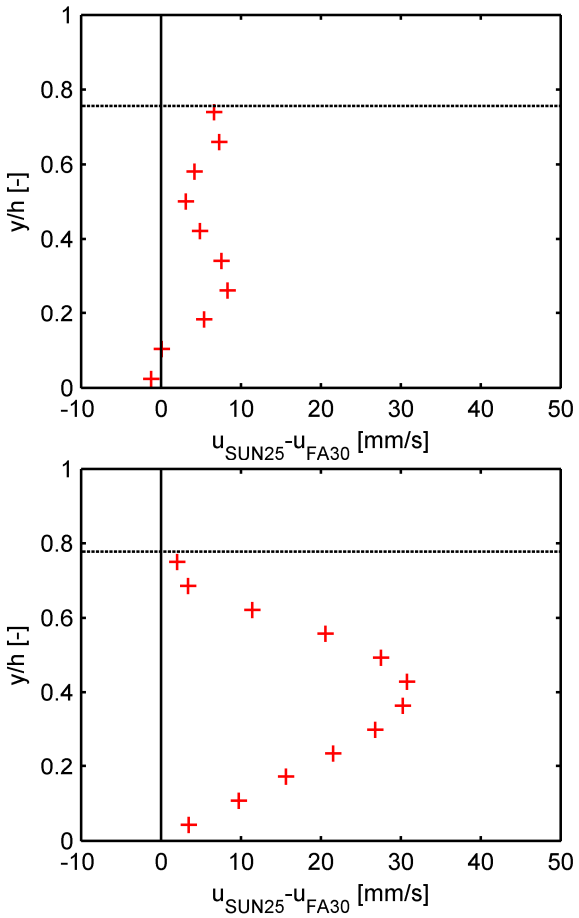



**Figure 11.** Distribution of local slip velocity between fractions SUN25 and FA30 across the transport layer in the tilting flume. **Upper plot**: test no. 1, **lower plot**: test no. 2. Legend: red marker—experimental $u_{SUN25} - u_{FA30}$, horizontal dash line—visually estimated top of the transport layer.

In nearly horizontal flows, estimations of both the local slip and average slip are more challenging than in corresponding vertical flows where the slip velocity is simply related to the hindered settling velocity of the particles. A method for estimating the average slip in the flow cross-section using the measured velocity distributions is discussed below. Moreover, the discussion includes an estimation of additional average (flow cross-section-averaged) quantities.

#### 3.2.3. Average Slip Velocity between Phases and Discussion of the Use of Velocity Distributions for Experimental Characterization of Granular Flow in Flume

The measured velocity distributions offer valuable insights into important quantities for the experimental characterization of granular flow above a mobile bed in the flume. These quantities encompass the flow rates of the solid–liquid mixture and its phases, the average velocities of the mixture and its two phases, and the corresponding average slip between phases in the flow.

To exemplify the application of the measured velocity distributions, we introduce a straightforward granular flow evaluation method. This method assumes negligible slip between the two fractions of solids and a linear distribution of the bimodal mixture solids across the transport layer above the mobile bed. The simplifying assumption of the linear distribution of solids is justified by previous measurements of SUN25 solid distributions in the flume.

This method utilizes the measured solids flow rate as a reliable input parameter, obtained through two independent measuring methods. Additionally, the observed elevations of the top of the bed, the transport layer, and the water surface are considered as inputs. Further inputs include the distribution of the solids' velocity measured within the transport layer and the distribution of the water velocity measured between the top of the bed and the water surface.

In the initial step, the local velocities of the solids are approximated using a polynomial function to generate the local velocities at all the positions within the transport layer, including the boundary values at the top and bottom of the transport layer. Additionally, the local values of the solid concentrations, c, are estimated at these boundaries, and a linear distribution is assumed between them. Numerical integration of the product of velocity distribution and solid distribution, $u_s \cdot c$, over the cross-sectional area of the transport layer yields the solids' flow rate, $Q_s$, which is then compared to the measured solids' flow rate. The boundary values of the concentration at the top and bottom of the transport layer are chosen so that the integrated flow rate matches the measured one.

In the subsequent step, the measured distribution of the water velocity, $u_f$, is approximated by a polynomial function, and the product $u_f \cdot (1 - c)$ is integrated over the flow cross-sectional area, A, to obtain the flow rate of water, $Q_f$. The sum of $Q_f$ and $Q_s$ gives the total flow rate through the flume, $Q_m = Q_f + Q_s$.

Finally, the solids' distribution is integrated over the flow cross-sectional area, yielding the average volumetric spatial concentration of the solids, $C_{vi}$. This allows us to distinguish between the average velocity of the solids, $v_s = Q_s/(C_{vi} \cdot A)$, and the average velocity of the water, $v_f = Q_f/([1 - C_{vi}] \cdot A)$. The average velocity of the solid–water mixture is $v_m = Q_m/A$. The average slip velocity between the phases is $v_f - v_s$, and it must be greater than the unity for nearly horizontal granular flow in a flume. Additional parameters can be used to quantify the average slip in granular flows. The delivered volumetric concentration $C_{vd}$, defined as $C_{vd} = Q_s/Q_m$, is directly related to the spatial concentration $C_{vi}$ through $C_{vd} = C_{vi} \cdot v_s/v_m$. It shows that the delivered concentration must be less than the spatial value, because $v_s$ is less than $v_m$.

The previously mentioned relations are employed in the evaluation method to predict the average quantities using the measured velocity distributions of the solids and liquid. The values of the predicted average quantities are summarized in Table 5 and exhibit good agreement with the experimentally determined average quantities of $Q_f$, $Q_m$, and $C_{vd}$ using independent measuring techniques (for comparison, see Table 4). These results not only quantify the average slip velocity between phases ($v_f - v_s$) in the nearly horizontal flow but also confirm that the average slip velocity is significantly higher than in the vertical granular flow.

**Table 5.** Cross-section-averaged quantities evaluated using the measured velocity distributions.

| Quantity [Unit] | Test No. 1 | Test No. 2 |
|---|---|---|
| Flow rate of water $Q_f$ [L/s] | 5.76 | 5.87 |
| Flow rate of solids $Q_s$ [L/s] | 0.42 | 0.70 |
| Total flow rate $Q_m$ [L/s] | 6.18 | 6.57 |
| Average velocity of water $v_f$ [m/s] | 0.827 | 0.860 |
| Average velocity of solids $v_s$ [m/s] | 0.341 | 0.322 |
| Average velocity of solid–liquid mixture $v_m$ [m/s] | 0.754 | 0.730 |
| Average slip velocity between phases $v_f - v_s$ [m/s] | 0.486 | 0.538 |
| Delivered concentration $C_{vd}$ [−] | 0.068 | 0.106 |
| Average spatial concentration $C_{vi}$ [−] | 0.151 | 0.241 |

In conclusion, the tests demonstrated the presence of the local slip velocity between the transported particles of the two fractions of different sizes at all elevations in the flow of a bimodal mixture above the bed in a nearly horizontal open-channel flow. Its magnitude is of the same order as the local slip velocity between the fractions in the vertical flow. The local

slip velocity between the particles and the carrying water is also of a comparable magnitude. However, In contrast to the vertical flow, the cross-section averaged slip velocity between the particles and water is considerably larger due to the flow stratification in the nearly horizontal flow, resulting in a significantly higher average spatial concentration $C_{vi}$ than the corresponding delivered concentration $C_{vd}$.

For open-channel flows with intense sediment transport, the high $C_{vi}$ resulting from slip between phases has significant consequences. It increases the shear stress acting on the top of the mobile granular bed, impacting bed friction and erosion at the top of the granular bed.

**Author Contributions:** Conceptualization, L.S. and V.M.; methodology, L.S., T.P. and V.M.; experiment, L.S. and T.P.; data analysis, L.S., T.P. and V.M.; writing—original draft preparation, L.S., T.P., V.M., L.S., T.P. and V.M.; supervision, V.M.; project administration, V.M.; funding acquisition, V.M. All authors have read and agreed to the published version of the manuscript.

**Funding:** This research was funded by the Czech Science Foundation, grant number 23-07772S, and by the Czech Technical University student grant OHK1-021/23.

**Data Availability Statement:** Data is contained within the article.

**Conflicts of Interest:** The authors declare no conflicts of interest. The funders had no role in the design of the study; in the collection, analyses, or interpretation of data; in the writing of the manuscript; or in the decision to publish the results.

## References

1. Paterson, A.J.C. Pipeline transport of high density slurries: A historical review of past mistakes, lessons learned and current technologies. *Min. Technol.* **2012**, *121*, 37–45. [CrossRef]
2. van den Berg, C.H. *IHC Merwede Handbook for Centrifugal Pumps and Slurry Transportation*; MTI Holland: Kinderdijk, The Netherlands, 2013.
3. van Wijk, J.M.; Talmon, A.M.; van Rhee, C. Stability of vertical hydraulic transport processes for deep ocean mining: An experimental study. *Ocean Eng.* **2016**, *125*, 203–213. [CrossRef]
4. Talmon, A.M. Analytical model for pipe wall friction of pseudo-homogenous sand slurries. *Part. Sci. Technol.* **2013**, *31*, 264–270. [CrossRef]
5. Spelay, R.; Gillies, R.G.; Hashemi, S.A. Kinematic friction of concentrated suspensions of neutrally buoyant coarse particles. In Proceedings of the 20th International Conference on Hydrotransport, Melbourne, Australia, 3–5 May 2017.
6. Visintainer, R.; Matoušek, V.; Pullum, L.; Sellgren, A. *Slurry Transport Using Centrifugal Pumps*, 4th ed.; Springer Nature: Cham, Switzerland, 2023. [CrossRef]
7. Revil-Baudard, T.; Chauchat, J.; Hurther, D.; Barraud, P.-A. Investigation of sheet-flow processes based on novel acoustic high-resolution velocity and concentration measurements. *J. Fluid Mech.* **2015**, *767*, 1–30. [CrossRef]
8. Matoušek, V.; Bareš, V.; Krupička, J.; Picek, T.; Zrostlík, Š. Experimental investigation of internal structure of open-channel flow with intense transport of sediment. *J. Hydrol. Hydromech.* **2015**, *63*, 318–326. [CrossRef]
9. Fromant, G.; Mieras, R.S.; Revil-Baudard, T.; Puleo, J.A.; Hurther, D.; Chauchat, J. On bedload and suspended load measurement performances in sheet flows using acoustic and conductivity profilers. *J. Geophys. Res. Earth Surf.* **2018**, *123*, 2546–2562. [CrossRef]
10. Guta, H.; Hurther, D.; Chauchat, J. Bedload and concentration effects on turbulent suspension properties in heavy particle sheet flows. *J. Hydraul. Eng.* **2022**, *148*, 04022012. [CrossRef]
11. Armanini, A.; Capart, H.; Fraccarollo, L.; Larcher, M. Rheological stratification in experimental free-surface flows of granular-liquid mixtures. *J. Fluid Mech.* **2005**, *532*, 269–319. [CrossRef]
12. Larcher, M.; Fraccarollo, L.; Armanini, A.; Capart, H. Set of measurement data from flume experiments on steady uniform debris flows. *J. Hydraul. Res.* **2007**, *45*, 59–71. [CrossRef]
13. Capart, H.; Fraccarollo, L. Transport layer structure in intense bed-load. *Geophys. Res. Lett.* **2011**, *38*, L20402. [CrossRef]
14. Matoušek, V.; Zrostlík, Š.; Fraccarollo, L.; Prati, A.; Larcher, M. Internal structure of intense collisional bed load transport. *Earth Surf. Process. Landf.* **2019**, *44*, 2285–2296. [CrossRef]
15. Gonzales-Odina, J.M.; Liu, P.L.-F.; Fraccarollo, L. Entrainment and adaptation processes in the evolution of collisional bedload layers. *Eur. J. Mech. B Fluids* **2022**, *92*, 132–142. [CrossRef]
16. Capart, H.; Young, D.L.; Zech, Y. Voronoi imaging methods for the measurement of granular flows. *Exp. Fluids* **2002**, *32*, 121–135. [CrossRef]
17. Spinewine, B.; Capart, H.; Larcher, M.; Zech, Y. Three-dimensional Voronoi imaging methods for the measurement of near-wall particulate flows. *Exp. Fluids* **2003**, *34*, 227–241. [CrossRef]
18. Matoušek, V.; Zrostlík, Š. Collisional transport model for intense bed load. *J. Hydrol. Hydromech.* **2020**, *68*, 60–69. [CrossRef]
19. Matoušek, V. Modelling intense combined load transport in open channel. *Water* **2022**, *14*, 572. [CrossRef]

20. Wilson, K.C.; Clift, R.; Addie, G.R.; Maffett, J. Effect of broad particle grading on slurry stratification ratio and scale-up. *Powder Technol.* **1990**, *61*, 165–172. [CrossRef]
21. Shook, C.A.; Gillies, R.; Haas, D.B.; Husband, W.H.W.; Small, M. Flow of coarse and fine sand slurries in pipelines. *J. Pipelines* **1982**, *3*, 13–21.
22. Gillies, R.G.; Shook, C.A. Modelling high concentration slurry flows. *Can. J. Chem. Eng.* **2000**, *78*, 709–716. [CrossRef]
23. Maciejewski, W.; Oxenford, J.; Shook, C.A. Transport of coarse rock with sand and clay slurries. In Proceedings of the 12th Hydrotransport, Brugge, Belgium, 28–30 September 1993; pp. 705–724.
24. Kaushal, D.R.; Sato, K.; Toyota, T.; Funatsu, K.; Tomita, Y. Effect of particle size distribution on pressure drop and concentration profile in pipeline flow of highly concentrated slurry. *Int. J. Multiph. Flow.* **2005**, *31*, 809–823. [CrossRef]
25. Kumar, U.; Singh, S.N.; Seshadri, V. Prediction of flow characteristics of bimodal slurry in horizontal pipe flow. *Part. Sci. Technol.* **2008**, *26*, 361–379. [CrossRef]
26. Matoušek, V.; Chára, Z.; Konfršt, J.; Novotný, J. Experimental investigation on effect of stratification of bimodal settling slurry on slurry flow friction in pipe. *Exp. Therm. Fluid Sci.* **2022**, *132*, 110561. [CrossRef]
27. Iseya, F.; Ikeda, H. Pulsations in bedload transport rates induced by longitudinal sediment sorting: A flume study using sand and gravel mixtures. *Geogr. Ann. Ser. A* **1987**, *69*, 15–27. [CrossRef]
28. Ferguson, R.I.; Prestegaard, K.L.; Ashworth, P.J. Influence of sand on hydraulics and gravel transport in a braided gravel bed river. *Water Resour. Res.* **1989**, *25*, 635–643. [CrossRef]
29. Wilcock, P.R.; Kenworthy, S.T.; Crowe, J.C. Experimental study of the transport of mixed sand and gravel. *Water Resour. Res.* **2001**, *37*, 3349–3358. [CrossRef]
30. Curran, J.C.; Wilcock, P.R. Effect of sand supply on transport rates in a gravel-bed channel. *J. Hydraul. Eng.* **2005**, *131*, 961–967. [CrossRef]
31. Hill, K.M.; Gaffney, J.; Baumgardner, S.; Wilcock, P.R.; Paola, C. Experimental study of the effect of grain sizes in a bimodal mixture on bed slope, bed texture, and the transition to washload. *Water Resour. Res.* **2017**, *53*, 923–941. [CrossRef]
32. Dudill, A.; Lafaye de Micheaux, H.; Frey, P.; Church, M. Introducing finer grains into bedload: The transition to a new equilibrium. *J. Geophys. Res. Earth Surf.* **2018**, *123*, 2602–2619. [CrossRef]
33. Dudill, A.; Venditti, J.G.; Church, M.; Frey, P. Comparing the behaviour of spherical beads and natural grains in bedload mixtures. *Earth Surf. Process. Landf.* **2020**, *45*, 831–840. [CrossRef]
34. Zrostlík, Š.; Matoušek, V. On the effect of segregation on intense bimodal bed load. *EPJ Web Conf.* **2017**, *143*, 02148. [CrossRef]
35. Matoušek, V.; Krupička, J.; Picek, T.; Svoboda, L. Segregation in bimodal contact/combined load: Tilting-flume study. In Proceedings of the 20th International Conference on Transport & Sedimentation of Solid Particles, Wroclaw, Poland, 26–29 September 2023. [CrossRef]
36. Svoboda, L.; Picek, T.; Matoušek, V. Camera-measured velocity distribution in laboratory open-channel flow with intense transport of bimodal combined-load. *J. Hydrol. Hydromech.* **2023**, *71*, 331–340. [CrossRef]
37. Rebai, D.; Berzi, D.; Ballio, F.; Matoušek, V. Experimental comparisons of inclined flows with and without intense sediment transport: Flow resistance and surface elevation. *J. Hydraul. Eng.* **2022**, *148*, 04022026. [CrossRef]
38. Haider, A.; Levenspiel, O. Drag coefficient and terminal velocity of spherical and non-spherical particles. *Powder Technol.* **1989**, *58*, 63–70. [CrossRef]
39. Richardson, J.F.; Zaki, W.N. Sedimentation and fluidisation: Part 1. *Trans. Inst. Chem. Eng.* **1954**, *32*, S82–S100. [CrossRef]


**Disclaimer/Publisher's Note:** The statements, opinions and data contained in all publications are solely those of the individual author(s) and contributor(s) and not of MDPI and/or the editor(s). MDPI and/or the editor(s) disclaim responsibility for any injury to people or property resulting from any ideas, methods, instructions or products referred to in the content.